

Article

Numerical Study on Thermal Hydraulic Performance of Supercritical LNG in Zigzag-Type Channel PCHEs

Zhongchao Zhao *, Yimeng Zhou, Xiaolong Ma, Xudong Chen, Shilin Li and Shan Yang

School of Energy and Power, Jiangsu University of Science and Technology, Zhenjiang 212000, China; ymzhou@stu.just.edu.cn (Y.Z.); marlon@stu.just.edu.cn (X.M.); xudongchen@stu.just.edu.cn (X.C.); shilinli@stu.just.edu.cn (S.L.); shanyang33@stu.just.edu.cn (S.Y.)

* Correspondence: zhongchaozhao@just.edu.cn; Tel.: +86-0511-8449-3050

Received: 18 December 2018; Accepted: 4 February 2019; Published: 11 February 2019



Abstract: In this paper, we study a promising plate-type heat exchanger, the printed circuit heat exchanger (PCHE), which has high compactness and is suitable for high-pressure conditions as a vaporizer during vaporization. The thermal hydraulic performance of supercritical produce liquefied natural gas (LNG) in the zigzag channel of PCHE is numerically investigated using the SST κ - ω turbulence model. The thermo-physical properties of supercritical LNG from 6.5 MPa to 10MPa were calculated using piecewise-polynomial approximations of the temperature. The effect of the channel bend angle, mass flux and inlet pressure on local convection heat transfer coefficient, and pressure drop are discussed. The heat transfer and pressure loss performance are evaluated using the Nusselt and Euler numbers. Nu/Eu is proposed to evaluate the comprehensive heat transfer performance of PCHE by considering the heat transfer and pressure drop characteristics to find better bend angle and operating conditions. The supercritical LNG has a better heat transfer performance when bend angle is less than 15° with the mass flux ranging from $207.2 \text{ kg}/(\text{m}^2 \cdot \text{s})$ to $621.6 \text{ kg}/(\text{m}^2 \cdot \text{s})$, which improves at bend angle of 10° and lower compared to 15° at mass flux above $414.4 \text{ kg}/(\text{m}^2 \cdot \text{s})$. The heat transfer performance is better at larger mass flux and lower operating pressures.

Keywords: printed circuit heat exchanger; supercritical LNG; zigzag type; heat transfer performance

1. Introduction

Natural gas (NG) is an advantageous energy source for various applications due to its clean nature and its environmental and economic advantages [1]. NG is liquefied to produce liquefied natural gas (LNG) for long-distance transportation and storage, and is regasified before terminal utilization [2]. Therefore, an efficient and reliable LNG vaporizer is a key component in a LNG vaporization system. The common LNG vaporizers, such as intermediate fluid vaporizers, open rack vaporizers (ORVs), super ORVs and submerged combustion vaporizers [3–5] do not satisfy the requirement of high efficiency and compactness in finite volume vaporization processes. Hence, the printed circuit heat exchanger (PCHE), which is a prospective plate-type heat exchanger with high compactness that can operate under high pressure and low temperature, has been investigated by many researchers [6,7].

In recently years, four PCHE channel morphologies have been studied, namely the straight, zigzag, S-shape, and airfoil shapes. Figley et al. [8] conducted numerical simulations to investigate the thermal hydraulic performance of the straight-channel PCHE using helium. The thermal effectiveness and overall heat transfer coefficient were defined and calculated to describe the overall heat transfer performance of PCHE. Kim et al. [9] predicted the thermal performance by developing a mathematical expression of geometric parameters, material properties, and flow conditions to express the effectiveness of cross, parallel, and counterflow PCHEs. Yoon et al. [10] developed a friction factor and Nusselt number relationship of laminar flow in various bend angles for a semi-circular zigzag

channel PCHE. Ishizuk et al. [11] studied heat transfer and flow characteristics of zigzag-type PCHE experimentally using supercritical carbon dioxide and obtained the total heat transfer efficiency and pressure drop. Tsuzuki et al. [12] performed numerical analysis of the transition section of a zigzag-type channel PCHE, and encountered the presence of vortices and local circulation flow. Ngo et al. [13,14] conducted three-dimensional simulations of the pressure drop and Nusselt number of PCHEs with S-shaped fins in a supercritical carbon dioxide loop. Kim et al. [15] studied airfoil PCHEs using numerical analysis and indicated that the stream line was smooth and the vortices and countercurrents disappeared in the airfoil channel. Zhao et al. [16] investigated the heat transfer characteristics of an airfoil PCHE numerically using supercritical LNG and optimized the arrangement of airfoil fins.

In spite of the superior pressure drop performance of PCHEs with S-shaped and airfoil fins, compared to straight and zigzag-type PCHEs, discontinuous fins lack durability at high pressure operating conditions, which is attributed to the confined junction area of the fins in the diffuser bonding [17]. This in turn leads to an increase in manufacturing and maintenance costs [18,19]. Therefore, it makes sense to further investigate continuous channels and optimize channel shapes.

Previously, investigations were mainly concerned with the heat transfer performance and pressure drop of zigzag PCHEs, but few combined the heat transfer and pressure drop performance to study the optimization of zigzag PCHEs in terms of bend angle and operating conditions. In addition, supercritical fluids can be used to improve heat transfer performance due to their favorable properties, like high density, low viscosity, and high thermal conductivity compared to conventional fluids [20]. Most studies on the flow and heat transfer characteristics of fluids in PCHE have been conducted using helium and water [21–23], and many researchers also used supercritical water and supercritical carbon dioxide to investigate PCHEs [24,25]. However, studies on the heat transfer performance of supercritical LNG in zigzag PCHE under low temperature and high pressure conditions are rare [16].

In this study, the flow and heat transfer characteristics of supercritical LNG in zigzag-type PCHEs were numerically simulated at an operating pressure of 6.5–10 MPa. The effects of bend angle and mass flux on heat transfer performance were also investigated. The local convection heat transfer coefficient and pressure drop of supercritical LNG under different conditions are discussed. Dimensionless parameters such as the Nusselt number (Nu) and Euler number (Eu) are analyzed to assess the heat transfer and pressure loss performance, Nu/Eu of the bend angles and operating conditions are investigated by considering the performance of heat transfer and the pressure drop of supercritical LNG in PCHEs.

2. Numerical Approach

2.1. Physical Model and Boundary Conditions

In this study, the thermal hydraulic performance of supercritical LNG in zigzag PCHEs is investigated. The cross flow PCHE core model with a full length of 400 mm using supercritical LNG in the cold side and R22 in the hot side is shown in Figure 1a. The supercritical LNG and R22 flow in the semicircular channel with a diameter of 1.5 mm, the solid is composed of steel with thermal conductive coefficient of 16.27 W/(m·K). In this paper, we only study the performance of supercritical LNG in the cold channel. Considering that the cold side of the PCHE contains hundreds of channels, it is unrealistic to consider all the channels, and it is therefore necessary to simplify the cold channels' model. Supercritical LNG flows in parallel in each cold channel, so some assumptions on its flow in the cold side are made. The mass flux is the same in every channel, and there is no temperature difference and heat loss between neighboring channels. The flow of supercritical LNG is steady and uniformly distributed. Based on these assumptions, the cold channel can be simplified to a single model with a geometry of 2 mm × 1.75 mm. The cross-section of the fluid channel is semicircular with a diameter of 1.5 mm (Figure 1b). The bend angles α vary from 0° (which is a straight channel) to 45° (Figure 1c).

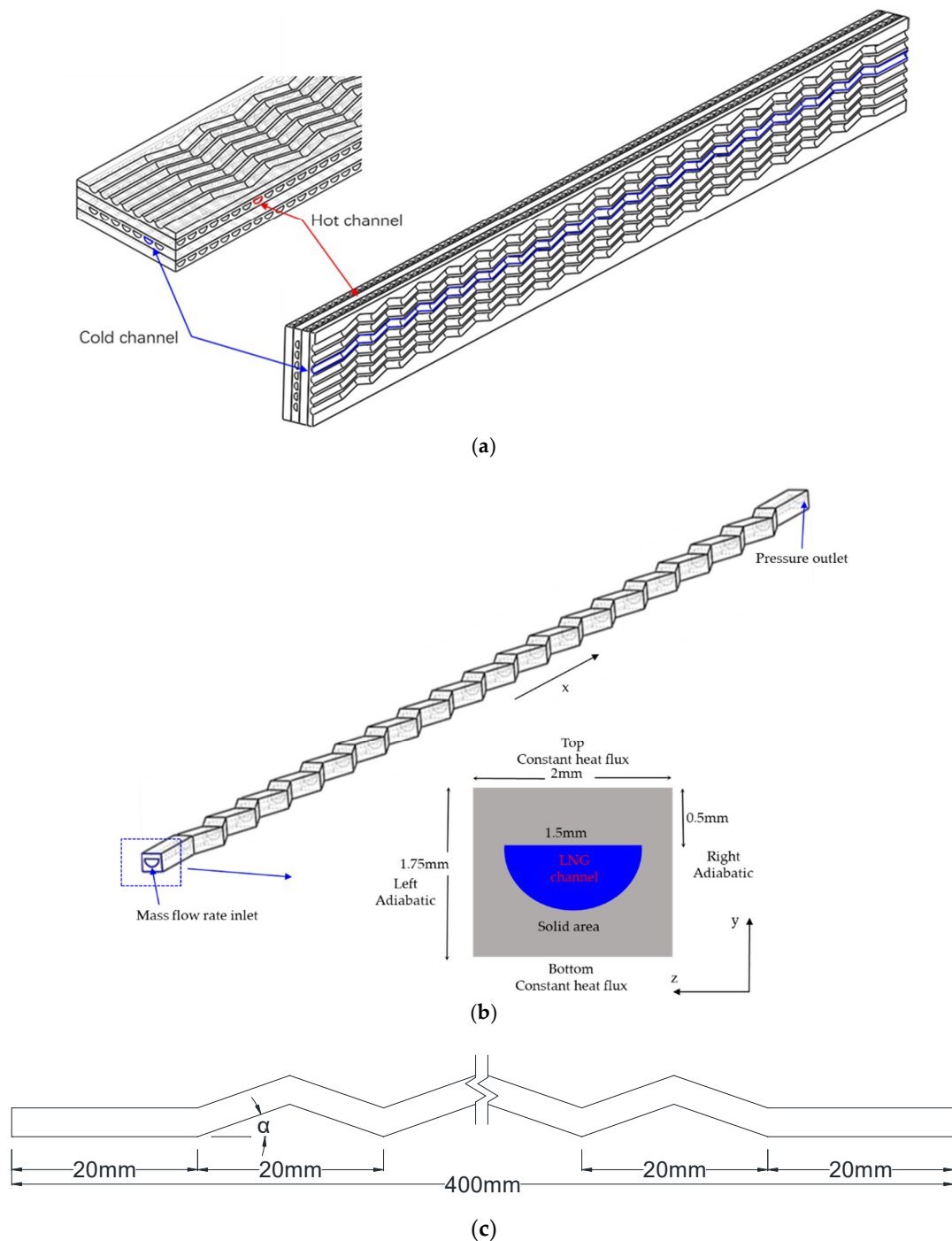


Figure 1. Schematic diagram of the physical model: (a) Schematic diagram of cross flow printed circuit heat exchanger (PCHE) model; (b) The computational single channel and boundary conditions; (c) Top view of zigzag channel.

The adjacent cold channels do not exhibit temperature difference and heat transfer loss; only the supercritical LNG in cold channels absorb heat from top and bottom hot channels. Three types of boundary conditions were applied in the model: fluid inlet, fluid outlet, and wall. The mass flow rate boundary condition was set at the inlet of the supercritical LNG channel whereas at the outlet the pressure-outlet boundary condition was applied (Figure 1b). The left and right walls of the single model are set to adiabatic boundary conditions, and the constant heat flux condition was used at top and bottom walls. The details of the boundary conditions are presented in Table 1.

Table 1. Boundary conditions in detail.

Inlet			Outlet	Left/Right Walls	Top/Bottom Walls
Pressure (MPa)	Temperature (K)	Mass flux (kg/m ² ·s)	Pressure outlet	Adiabatic	Constant heat flux (W/m ²)
10	121	207.2			7.5×10^4

2.2. Thermo-Physical Properties of Supercritical LNG

In this paper, the operating pressure of LNG considered varies from 6.5 MPa to 10 MPa, which is supercritical pressure. Supercritical LNG has gas-like properties, such as low viscosity, and liquid-like characteristics, like high density and high thermal conductivity. The thermo-physical properties of supercritical LNG, i.e., density, specific heat, thermal conductivity and viscosity, are affected by temperature and pressure. The properties' values were obtained from the NIST Standard Reference Database (REFPROP) [26]. For the numerical simulations, the temperature was changed from 121 K to 385 K. At such a large temperature difference, the properties of supercritical LNG change dramatically, using the average values will cause the inaccurate calculation results in ANSYS Fluent. Therefore, as shown in Figure 2, the thermal properties of supercritical LNG were approximated as piecewise-polynomial functions of temperature. The piecewise-polynomial functions of temperature at 10 MPa is shown in Table 2. The error percentages of various properties using the proposed approximation are shown in Figure 3. The errors were within $\pm 2.5\%$, which indicates the fitted piecewise-polynomial function approximations are suitable.

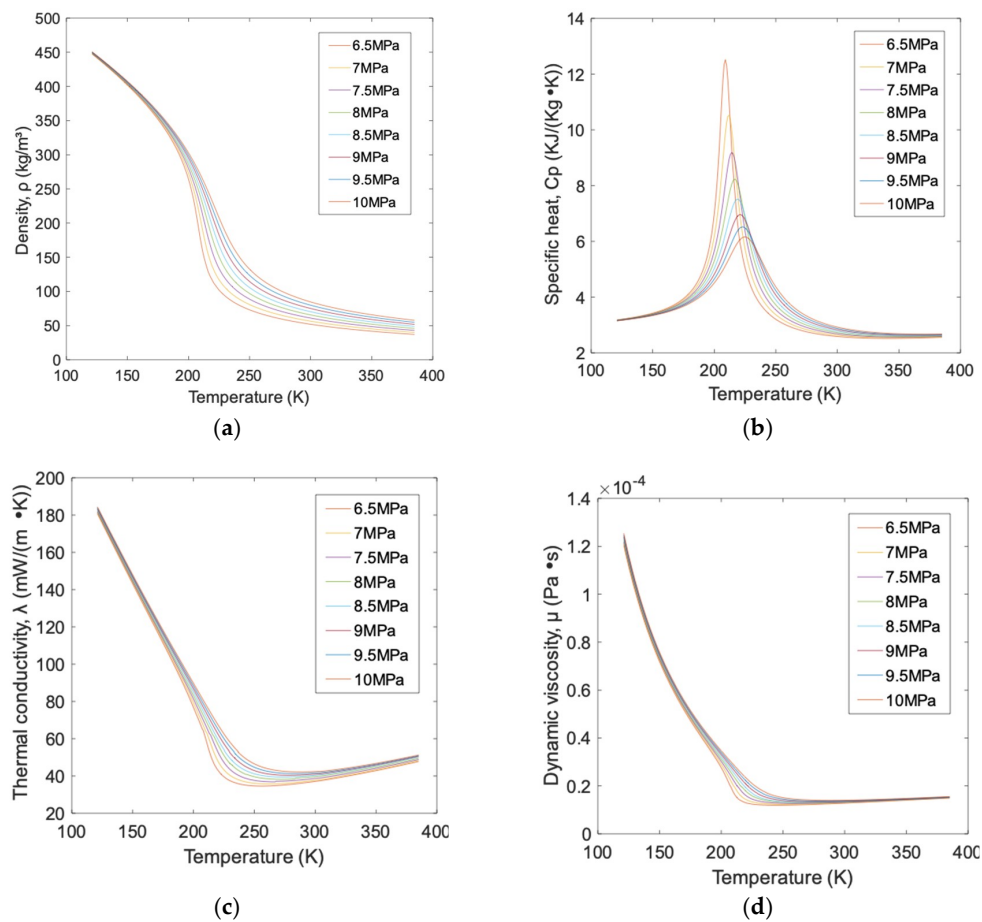
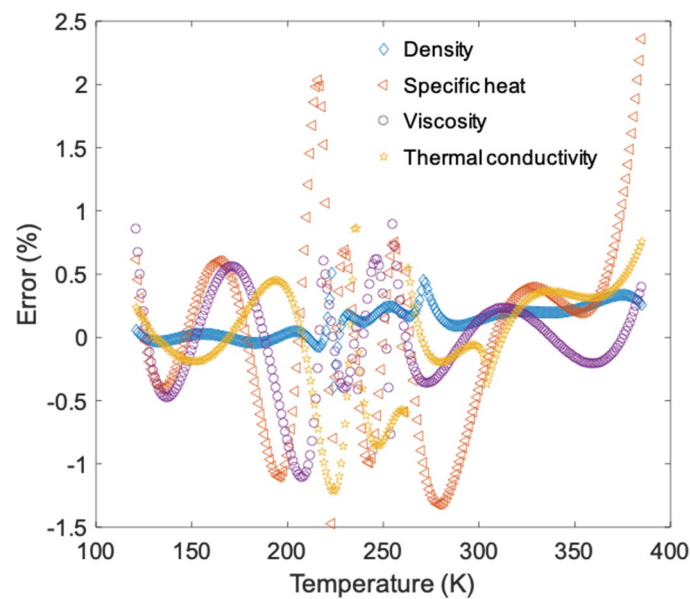


Figure 2. Thermo-physical properties of supercritical LNG at different pressures: (a) Density; (b) Specific heat; (c) Thermal conductivity; (d) Dynamic viscosity.

Table 2. Piecewise-polynomial functions at 10 MPa.

Temperature Range (K)	Density
121–223	$\rho = -1.29548 \times 10^{-6}T^4 + 7.459 \times 10^{-4}T^3 - 0.16537T^2 + 15.12763T - 2.45869$
223–271	$\rho = -5.30962 \times 10^{-4}T^3 + 0.43352T^2 - 119.03258T + 11,091.66885$
271–385	$\rho = 1.32923 \times 10^{-7}T^4 - 1.93454 \times 10^{-4}T^3 + 0.10675T^2 - 26.70158T + 2634.06161$
Specific Heat	
121–223	$c_p = 0.00436T^3 - 1.83425T^2 + 263.05475T - 9567.33957$
223–261	$c_p = 0.06448T^3 - 46.88971 \times 10^3T^2 + 11,278.86482T - 892,240.75366$
261–385	$c_p = -0.00111T^3 + 1.18621T^2 - 423.72673T + 53,206.50774$
Thermal Conductivity	
12–235	$\lambda = 1.07039 \times 10^{-8}T^3 - 4.35253 \times 10^{-6}T^2 - 6.44568 \times 10^{-4}T + 0.30675$
235–262	$\lambda = 7.96913 \times 10^{-6}T^2 - 0.00432T + 0.62882$
262–385	$\lambda = -6.69403 \times 10^{-9}T^3 + 7.36829 \times 10^{-6}T^2 - 0.00258 \times 10^{-2}T + 0.33402$
Viscosity	
121–218	$\mu = -7.71822 \times 10^{-11}T^3 + 4.71489 \times 10^{-8}T^2 - 1.01809 \times 10^{-5}T + 8.02631 \times 10^{-4}$
218–254	$\mu = 6.9276 \times 10^{-9}T^2 - 3.52808 \times 10^{-6}T + 4.64105 \times 10^{-4}$
254–385	$\mu = -2.07823 \times 10^{-12}T^3 + 2.1834 \times 10^{-9}T^2 - 7.43585 \times 10^{-7}T + 9.67009 \times 10^{-5}$

**Figure 3.** Error curves of linear interpolation functions.

2.3. Numerical Method and Grid Independence

The commercial software FLUENT was used to solve the 3D numerical model. Considering the inlet parameters, the flow corresponded to turbulent flow regimes. Some turbulence models have been studied and used in the literature; these include the κ - ϵ standard model, the RNG κ - ϵ model, the shear-stress transport (SST) κ - ω model and the low Reynolds number turbulence model [27,28]. In this study, the SST κ - ω model was used because of its more accurate results on heat transfer of supercritical fluids [29–32].

The governing equations for heat transfer were the continuity, momentum, and energy equations, respectively:

Continuity equation:

$$\frac{\partial}{\partial x_i}(\rho u_i) = 0, \quad (1)$$

where ρ is the density, and u_i is the velocity vector.

Momentum equation:

$$\frac{\partial}{\partial x_i}(\rho u_i u_j) = -\frac{\partial p}{\partial x_i} + \rho g_i + \frac{\partial}{\partial x_j}[(\mu + \mu_t) \frac{\partial u_i}{\partial x_j}], \quad (2)$$

where p is the pressure, μ and μ_t are the molecular and turbulent viscosities, respectively.

Energy equation:

$$\frac{\partial}{\partial x_i}(u_i(\rho E + p)) = \frac{\partial}{\partial x_i} \left(k_{eff} \frac{\partial T}{\partial x_i} + u_i \tau_{ij} \right), \quad (3)$$

where k_{eff} is effective conductivity, $k_{eff} = k + k_t$, and k_t is the turbulent thermal conductivity.

The transport equations are expressed as follows:

$$\frac{D(\rho\kappa)}{Dt} = \frac{\partial}{\partial x_j} \left[(\mu + \sigma_\kappa \mu_t) \frac{\partial \kappa}{\partial x_j} \right] + \tau_{ij} \frac{\partial u_i}{\partial x_j} - \beta^* \rho \omega \kappa \quad (4)$$

$$\frac{D(\rho\omega)}{Dt} = \frac{\partial}{\partial x_j} \left[(\mu + \sigma_{\omega 1} \mu_t) \frac{\partial \omega}{\partial x_j} \right] + \frac{\gamma}{\nu_t} \tau_{ij} \frac{\partial u_i}{\partial x_j} - \beta \rho \omega^2 + 2(1 - F_1) \rho \sigma_{\omega 2} \frac{1}{\omega} \frac{\partial \kappa}{\partial x_j} \frac{\partial \omega}{\partial x_j} \quad (5)$$

$$\omega = \frac{\varepsilon}{\beta^* \kappa}; \nu_t = \frac{a_1 \kappa}{\max(a_1 \omega; \Omega F_2)} \quad (6)$$

$$F_1 = \tan h(\arg_1^4); F_2 = \tan h(\arg_2^2) \quad (7)$$

$$\arg_1 = \min \left(\max \left(\frac{\sqrt{\kappa}}{0.09 \omega y}; \frac{500 \nu}{y^2 \omega} \right); \frac{4 \rho \sigma_{\omega 2} \kappa}{CD_{\kappa \omega} y^2} \right); CD_{\kappa \omega} = \max \left(2 \frac{\rho \sigma_{\omega 2}}{\omega} \frac{1}{\omega} \frac{\partial \kappa}{\partial x_j} \frac{\partial \omega}{\partial x_j}, 10^{-20} \right) \quad (8)$$

$$\arg_2 = \max \left(2 \frac{\sqrt{\kappa}}{0.09 \omega y}; \frac{500 \nu}{y^2 \omega} \right) \quad (9)$$

where ε is the turbulent kinetic energy dissipation rate, Ω is vorticity, and y is the distance from the wall. The constants and damping functions of the SST κ - ω model are shown in Table 3.

Table 3. Constants and functions used in the shear-stress transport (SST) model.

	$\sigma_{\omega 1}$	$\sigma_{\omega 2}$	κ	α_1	β^*
SST	0.5	0.865	0.41	0.31	0.09

The local convective heat transfer coefficient was calculated using Equation (10):

$$h = \frac{q}{T_w - T_b} = \frac{q}{T_w - (T_{out} + T_{in})/2}, \quad (10)$$

where q is the constant heat flux from the top and bottom walls, T_w is the wall temperature and T_b is average temperature of the inlet and the outlet.

Nu was defined as:

$$Nu = \frac{h D_h}{\lambda}; D_h = 4A/l \quad (11)$$

where D_h is the hydraulic diameter and λ is the local thermal conductivity of LNG, A is the cross-sectional area of the semicircular fluid channel and l is the circumference of the semicircular fluid channel section.

The local Fanning friction coefficient (f) was defined in terms of the pressure drop and is expressed by Equation (12):

$$f = \frac{\Delta P_f D_h}{2L \rho_b v_b^2}, \quad (12)$$

$$\Delta P_f = \Delta P - \Delta P_a = \Delta P - \left(\rho_{out} v_{out}^2 - \rho_{in} v_{in}^2 \right), \quad (13)$$

where ΔP is the total pressure and was obtained from Fluent directly, ΔP_f and ΔP_a are the frictional and accelerated pressure drops, respectively, L is the channel length, ρ_b and v_b are the bulk density and velocity of LNG, respectively.

The Reynolds number (Re) is given by Equation (14):

$$Re = \frac{\rho_b v_d D_h}{\mu_b}, \quad (14)$$

The Euler number (Eu) is defined as Equation (15):

$$Eu = \frac{\Delta P}{\rho_b v_b^2 / 2}, \quad (15)$$

For the solution methods, the SIMPLE algorithm was applied to establish the coupling of velocity and pressure. The momentum, turbulent kinetic energy, turbulent dissipation rate and energy were discretized using the second order upwind scheme. The calculation was considered to converge when the residuals were less than 10^{-6} .

The mesh on the computational domain was generated using GAMBIT. The grid independence was verified to confirm numerical result accuracy. The mesh size of solid, fluid and boundary layer's scale in fluid affect the grid numbers. The influence of the grid numbers on the convective heat transfer coefficient is shown in Table 4. Case 4 has a larger relative error compared to the other cases. The heat transfer coefficient in Cases 1, 2, and 3 is nearly the same. The relative error of the heat transfer coefficient between Cases 1 and 7 is only 0.08%. Therefore, considering the calculation accuracy and time, the 2,988,329 grid nodes (Case 1), showing in Figure 4, was selected in the present work.

Table 4. Boundary layers study.

Case	Scale of Boundary Layer	Rows of Boundary Layer	Cells of Nodes	Heat Transfer Coefficient W/(m ² ·K)	Relative Error (%)
1	0.01	5	2,988,329	2678.57	3.4%
2	0.01	8	3,589,947	2680.44	3.47%
3	0.003	5	2,974,634	2678.32	3.4%
4	0.03	5	2,697,546	2669.23	3.04%
5			815,644	2590.42	0
6	0.01	5	1,962,788	2636.39	1.8%
7			4,456,851	2680.62	3.48%

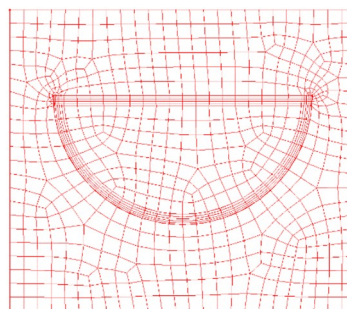


Figure 4. Cross section of computational grids.

2.4. Model Validation

To validate the accuracy and reliability of the model, the simulation results of temperature difference and pressure drop were compared to previous experimental results [30]. The experimental setup is shown in Figure 5. Since LNG is flammable and explosive, the straight-channel cross flow PCHE used supercritical nitrogen as the cold side fluid and R22 as the hot side fluid. The length of

the PCHE cold channel was 520 mm, the inlet temperature was 102 K, and the operating pressure varied from 6.5 MPa to 10 MPa. In the simulation, a straight channel model with a length of 520 mm was selected, which was the same as the experimental case. The boundary conditions are shown in Figure 1b. Supercritical nitrogen was used as the working fluid to confirm the correctness the experiment. The inlet pressure changed from 6.5 MPa to 10 MPa and the inlet temperature was 102 K. The comparison of temperature difference and pressure drop between simulation and experimental results is listed in Table 5. The maximum errors of temperature difference and pressure drop are 2.1% and 10.25%, respectively. The simulation pressure drop was less than the experimental, which may be attributed to the following factors: (1) the channel was assumed to be smooth in the numerical study while the PCHE channel of the experiment was rough, (2) the header pressure drop of inlet and the outlet were neglected in the numerical study, but may have been large in the experiment, and (3) the deviation of temperature and pressure transmissions. The simulation results are in accordance with the experiment, illustrating that the simulation model and method were credible.

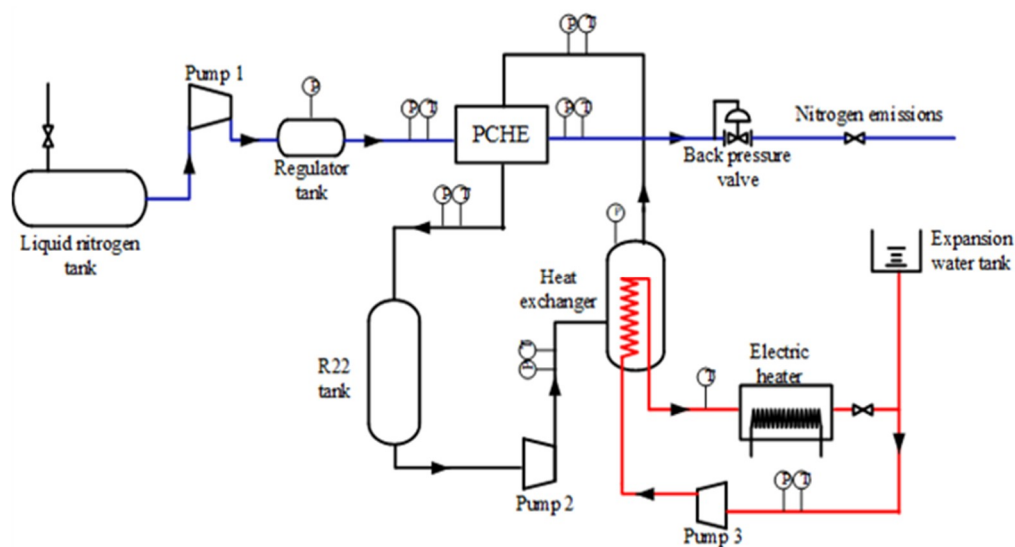


Figure 5. Schematic diagram of experimental setup.

Table 5. Relative error of simulation and experiment results.

Pressure (MPa)	Temperature Difference (K)		Relative Error (%)	Pressure Difference (Pa)		Relative Error (%)
	Experiment	Simulation		Experiment	Simulation	
6.5	178.9	175.1	2.1	16,612.35	15,167.36	10.25
7	180.3	178	1.27	15,636.09	14,521.4	9.95
7.5	182.1	180.4	0.94	14,742.24	14,071.62	7.05
8	182.6	182.3	0.16	13,847.55	13,188.32	6.62
8.5	183.5	184	0.27	13,035.22	12,504.69	6.81
9	185.7	185.5	0.11	12,156.68	11,810.66	4.70
9.5	186.1	185.8	0.16	11,342.33	10,862.6	4.42
10	186.6	186.4	0.11	10,578.6	10,189.45	3.82

3. Results and Discussion

Compared with traditional vaporizers, the heat transfer performance of PCHE is better, but the pressure drop is larger due to the small size of the channel, resulting in an increase of operating costs. A number of studies have shown that a supercritical fluid can enhance heat transfer and reduce pressure drop. The supercritical LNG vaporized by the PCHE is suitable for long distance transport and utilization. In this paper, the flow and heat transfer characteristics of supercritical LNG were

studied at 6.5–10 MPa, the performance of supercritical LNG at 10 MPa was discussed in detail in the following.

3.1. Effect of Bend Angles of the Zigzag Channel

The heat transfer performance of supercritical LNG is influenced significantly by the bend angle in the zigzag channel of a PCHE. The effect of the bend angles on the local convection heat transfer coefficient and bulk temperature of the LNG along the streamwise direction at a mass flux of $207.2 \text{ kg}/(\text{m}^2 \cdot \text{s})$ and operating pressure of 10 MPa are shown in Figure 6. As the bend angle increases, the local convection heat transfer coefficient and bulk temperature increase, which is due to the fact that with the increase of the bend angle, disturbance and turbulence will increase. Moreover, the local heat transfer coefficient increases and then decreases along the streamwise direction, and reaches a peak when the bulk temperature is near the pseudo-critical temperature at bend of 0° – 15° . This is because that the thermo-physical properties of supercritical LNG vary drastically at different temperatures, and the specific heat in particular reaches an extremum near the pseudo-critical temperature (Figure 2). However, at bend angles of 25° – 45° , the convection heat transfer coefficient is greater at $Np = 2$ – 4 . When the LNG flows into the channel, its velocity is not large in the $Np = 2$ – 4 . The flow separation is not dramatic and the velocity of vortices is not much different that of the fluid. As the flow develops, the velocity increases. The velocity difference of vortices and fluid becomes large and the vortices and flow separation increase (as shown in Figure 7b), leading to a decrease in the convection heat transfer coefficient. In addition, the heat transfer coefficient is larger at the inlet due to the entrance effect.

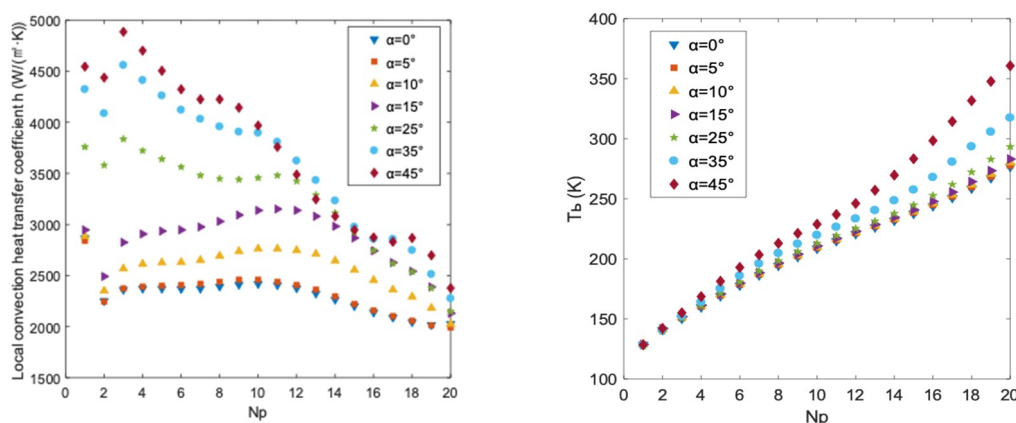


Figure 6. Local convection heat transfer coefficient and bulk temperature at different bend angles along the streamwise direction.

Figure 8 shows the pressure drop and Fanning friction coefficient (f) at different bend angles along the streamwise direction. The pressure drop increases with the bend angles and increases along the streamwise direction. The density and viscosity of the supercritical LNG decrease as the temperature increases (as shown in Figure 2a,d), resulting in a velocity increase and thus in pressure drop. Figure 7 shows the velocity vectors of different cross-sections along the channel and velocity vectors of $Np = 10$ – 12 at different bend angles. The velocity increases with the increase of bend angles, which is attributed to the increase of turbulence (Figure 7a). Flow separation and reverse flow appear in larger bend angles (Figure 7b), which increases flow resistance, resulting in an increased pressure drop. The velocity increases along the flow direction, which also increase the pressure drop along the streamwise. The Fanning friction coefficient f increases with the bend angle, which is the same trend observed in pressure drop. However, f decreases along the flow direction; this difference between pressure drop and f is due to the increase of velocity.

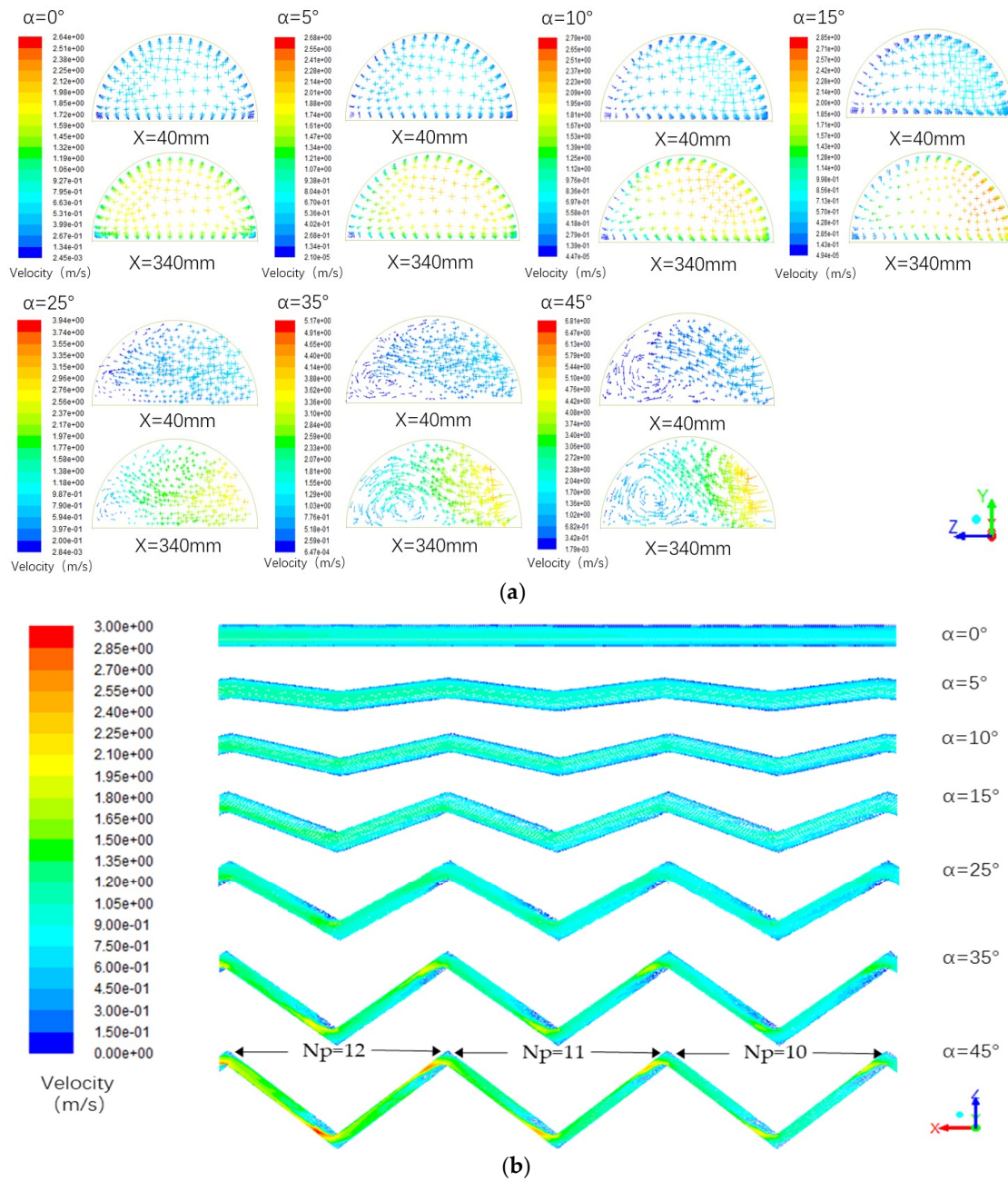


Figure 7. (a) Velocity vectors of different cross-sections along the channel with bend angles of 0° to 45° ; (b) Velocity vectors of $Np = 10\text{--}12$ at bend angles of 0° to 45° .

Figure 9 shows the Nusselt (Nu) and Euler (Eu) numbers along the streamwise direction at different bend angles. It can be seen that Nu increases with the bend angle, and reaches its maximum value near the pseudo-critical temperature, then decreases along the streamwise direction. This is because the thermal conductivity decreases intensely as the temperature rises before pseudo-critical temperature and rises slightly when the temperature surpasses the pseudo-critical value, reaching a minimum near the pseudo-critical temperature, which leads to a maximum for Nu near the pseudo-critical temperature. The Euler number increases as the bend angle rises, which is consistent with the change in pressure drop.

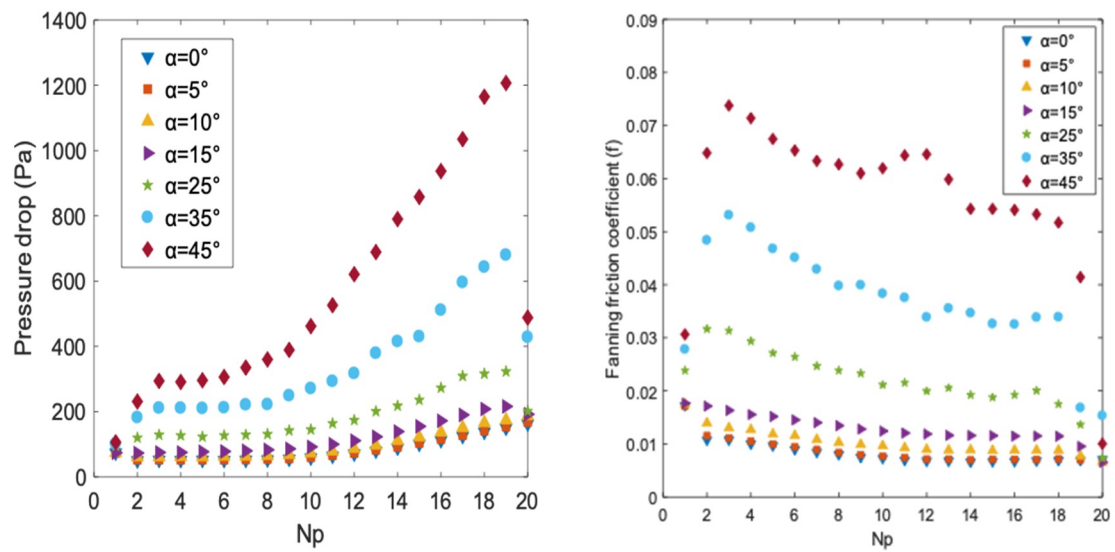


Figure 8. Pressure drop and fanning friction coefficient at different bend angles along the streamwise direction.

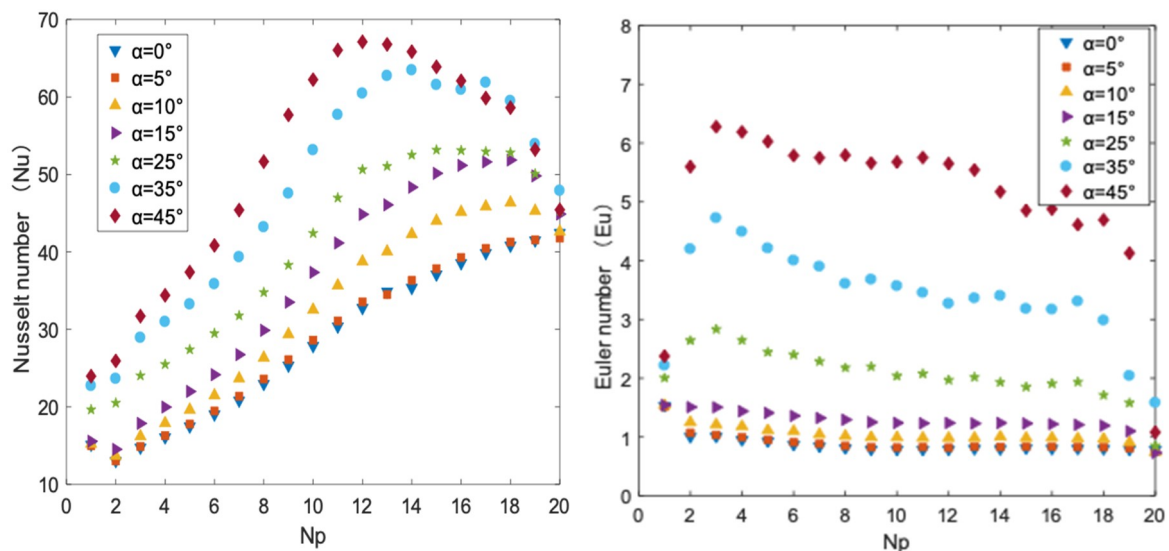


Figure 9. Local Nusselt number (Nu) and Euler (Eu) numbers at different bend angles along the streamwise direction.

The objective of improving the heat exchanger’s performance can be realized by increasing heat transfer performance and reducing pressure drop. It is therefore essential to comprehensively consider the heat transfer and pressure loss characteristics of supercritical LNG in PCHE. In this study, the ratio of Nusselt to Euler numbers (Nu/Eu) is proposed to evaluate the performance of supercritical LNG in the channel, where a larger ratio indicates better heat transfer performance. Figure 10 shows Nu/Eu at different bend angles. Nu/Eu reaches its peak value at a bend angle of 10° . When the bend angle exceeds 10° , the growth rate of Nu is much less than that of Eu. Nu and Eu at 0° and 5° are nearly the same, while from 5° to 10° , the increase of Nu is much greater than that of Eu.

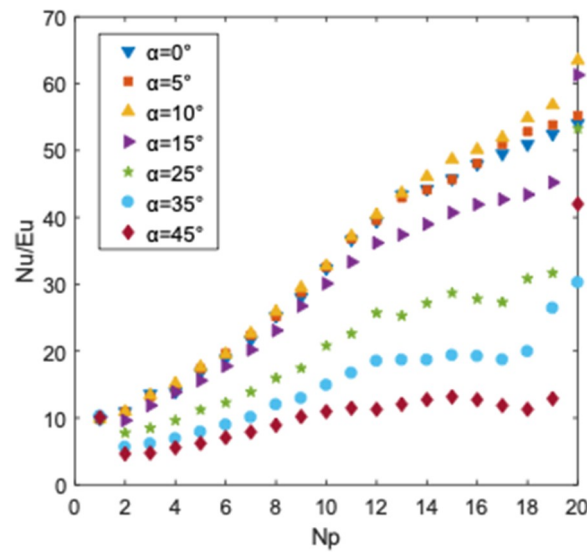


Figure 10. Nu/Eu at different bend angles along the streamwise direction.

3.2. Effect of Mass Flux

The effect of mass flux on flow and heat transfer performance of supercritical LNG was investigated at the bend angle of 10° and an operating pressure of 10 MPa. As shown in Figure 11, the local convective heat transfer coefficient and pressure drop increase significantly as the mass flux increases because of the enhancement of turbulent flow. When the mass flux is increased by 2 times, the local heat transfer coefficient increased 1.4 times, and at the same time, the pressure drop increases 3.3 times. The Nu and Eu are shown in Figure 12. The Nu increases as the mass flux is raised. However, at the last third of the channel, Nu peaks at a mass flux of 301.8 kg/(m²·s), and then decreases at further mass flux increase. This is because as mass flux is increased, the temperature of LNG decreases, its viscosity increases and its velocity decreases. When the heat flux is kept constant, the heat absorbed by the LNG per unit volume is reduced.

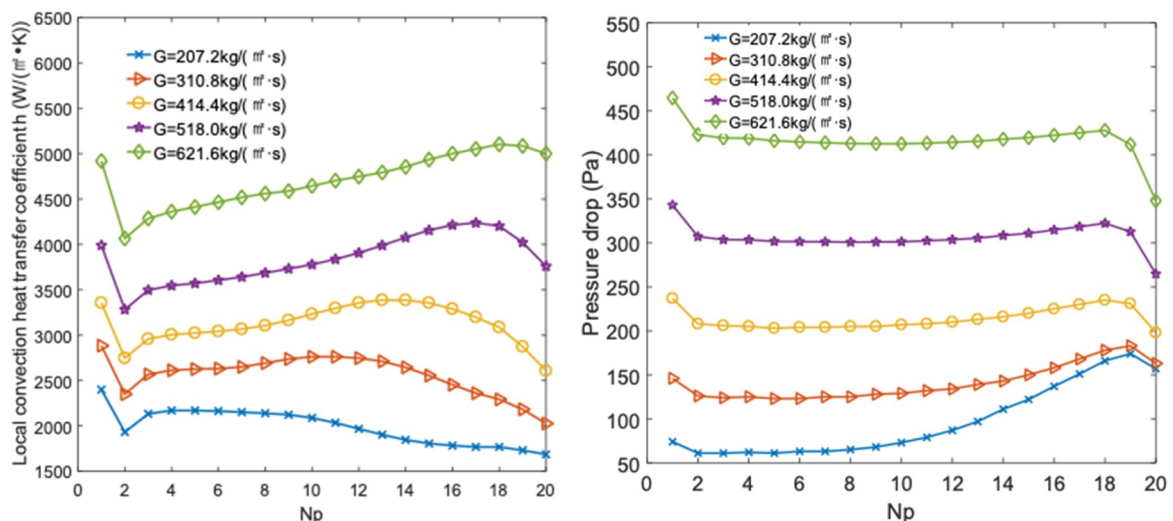


Figure 11. Effect of mass flux on local convection heat transfer coefficient and pressure drop along the streamwise direction.

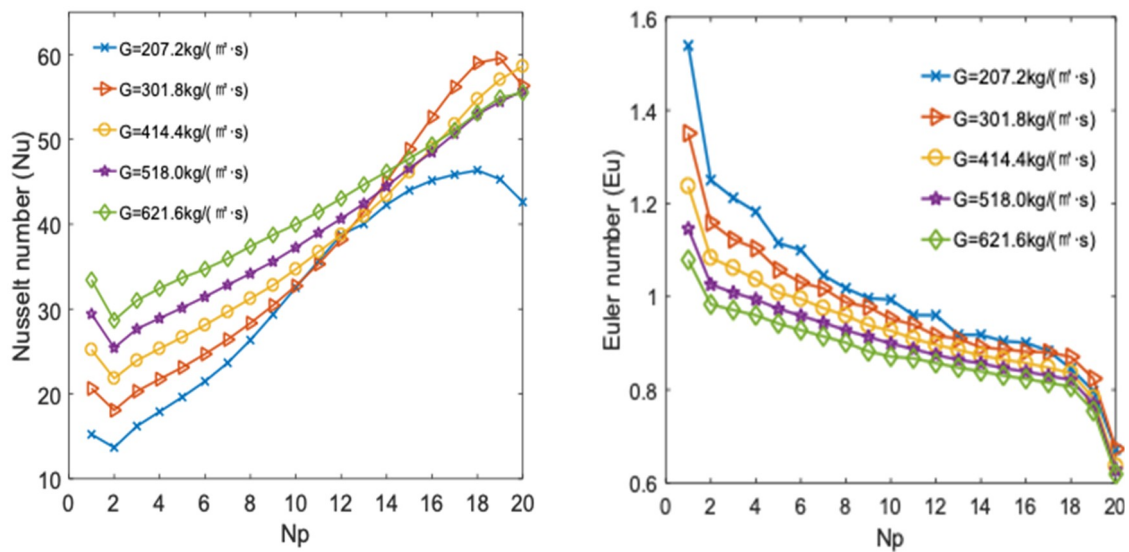


Figure 12. Effect of mass flux on Nu and Eu along the streamwise direction.

Eu increases as the mass flux decreases. The pressure drop and density increase as mass flux rises, but v_b^2 decreased. The increase rate of $\rho_b v_b^2$ is more than that of ΔP , which results in an increase of Eu as mass flux is reduced.

The influence of mass flux on Nu/Eu is shown in Figure 13. The Nu/Eu is increased as the mass flux is raised. However, at the last third of the channel, Nu/Eu peaks at a mass flux of 301.8 kg/(m²·s). The figure suggests that the heat transfer performance of the whole channel is improved as the mass flux increases, but with the development of the fluid flow, the local heat transfer performance is reduced at the last third of the channel, owing to the reduction of heat absorbed capacity by the unit volume fluid.

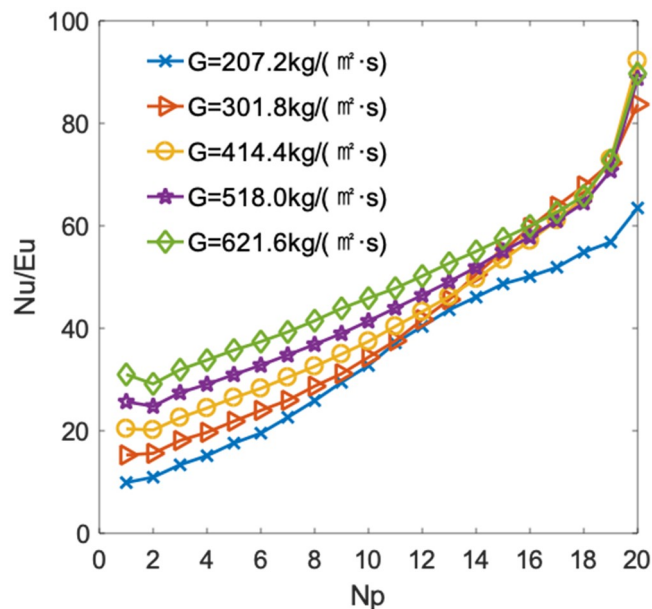


Figure 13. Effect of mass flux on Nu/Eu along the streamwise direction.

Figure 14 shows the impact of mass flux on Nu/Eu at different channel bend angles. The Nu/Eu is significantly reduced when the bend angle exceeds 15°, indicating that the increase of pressure drop is much higher than that of heat transfer performance. Consequently, the comprehensive heat transfer performance is not good when the bend angles exceeds 15°. When the mass flux varies

from $207.2 \text{ kg}/(\text{m}^2 \cdot \text{s})$ to $621.6 \text{ kg}/(\text{m}^2 \cdot \text{s})$, Nu/Eu are higher when the bend angle is less than 15° . However, Nu/Eu at bend angles of 10° and lower are increased compared to 15° at mass fluxes above $414.4 \text{ kg}/(\text{m}^2 \cdot \text{s})$. It can be concluded that the supercritical LNG in the PCHE has better heat transfer performance when the bend angle is less than 15° with the mass flux ranging from $207.2 \text{ kg}/(\text{m}^2 \cdot \text{s})$ to $621.6 \text{ kg}/(\text{m}^2 \cdot \text{s})$, and that it improves at bend angles of 10° and lower compared to 15° at mass fluxes above $414.4 \text{ kg}/(\text{m}^2 \cdot \text{s})$.

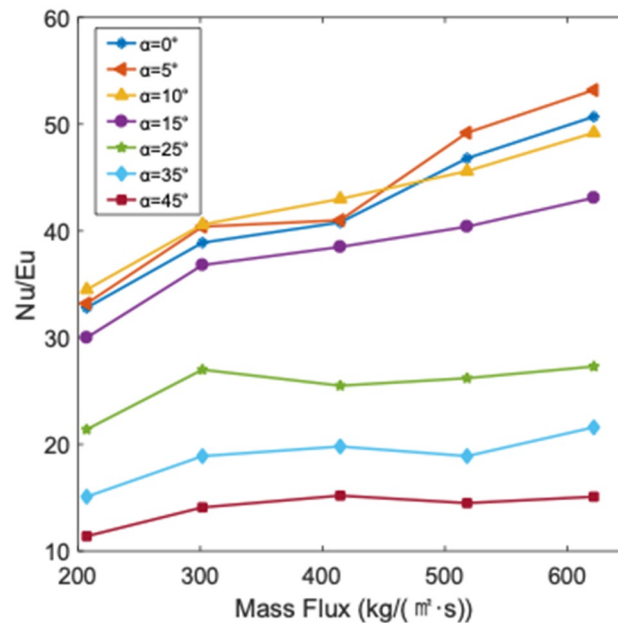


Figure 14. Effect of mass flux on Nu/Eu at different bend angles.

3.3. Effect of Inlet Pressure

At a bend angle of 10° and a mass flux of $207.2 \text{ kg}/(\text{m}^2 \cdot \text{s})$, the inlet pressure was varied from 6.5 MPa to 10 MP. The corresponding local heat transfer coefficient and pressure drop values are shown in Figure 15. Before the pseudo-critical temperature, the specific heat and thermal conductivity are slightly affected by the inlet pressure (as shown in Figure 2b,c), so the convection heat transfer coefficient changes slightly with the inlet pressure. After the pseudo-critical temperature, the inlet pressure effect on the local convective heat transfer coefficient is greater because of the specific heat is influenced by inlet pressure more. In addition, the reduction rate of the specific heat rises rapidly as the inlet pressure is reduced. Therefore, the local convection heat transfer coefficient decreases with the decrease of inlet pressure along the streamwise direction. This shows that the specific heat depends on inlet pressure and has a great influence on local convective heat transfer coefficient when temperature exceeds the pseudo-critical temperature.

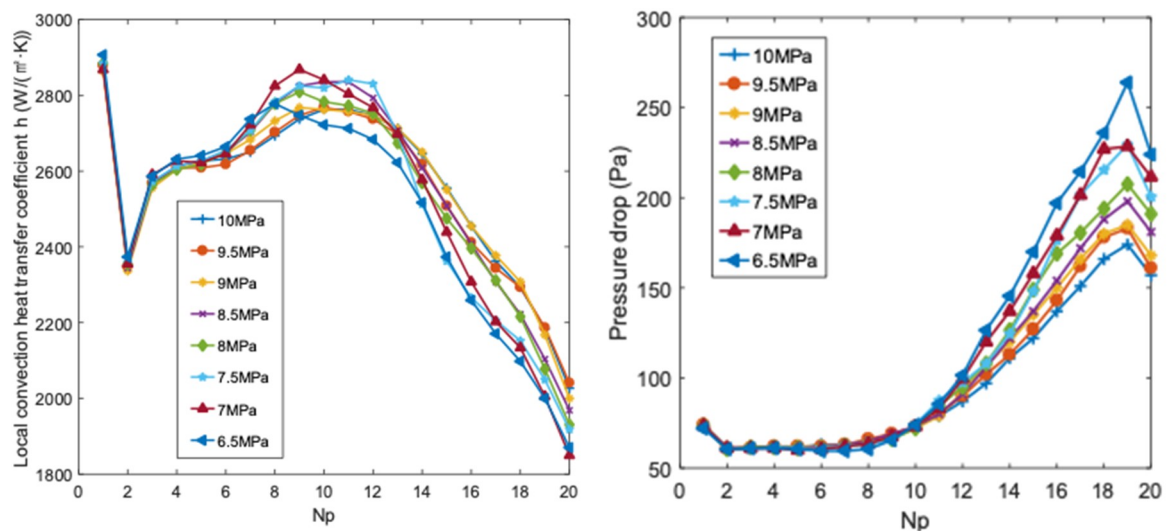


Figure 15. Effect of inlet pressure on local convection heat transfer coefficient and pressure drop along the streamwise direction.

With an increase of inlet pressure, the pressure drop decreases. As inlet pressure rises, the density and dynamic viscosity are larger (Figure 2a,d), which lowers the velocity of supercritical LNG. Hence, the pressure drop is reduced as the inlet pressure is increased. However, up until $Np = 10$, the pressure drop is uninfluenced by the changing inlet pressure. This is because the supercritical LNG has liquid-like properties, so the influence of inlet pressure on density and dynamic viscosity as well as velocity is small (as shown in Figure 2), which leads to pressure drop being only slightly effected by the inlet pressure. After $Np = 10$, the supercritical LNG has gas-like properties, so the influence of inlet pressure on density and dynamic viscosity is greater, leading to the large effect on velocity and causing the pressure drop to change more obviously with the inlet pressure. At the last portion of the channel, the pressure drop reduced, because the last pitch of the channel is straight, which reduces turbulence.

The effect of inlet pressure on Nu and Eu are shown in Figure 16, where both Nu and Eu decrease with as inlet pressure increased. Nu is inversely proportional to thermal conductivity, so as the inlet pressure increases, the thermal conductivity increased, which decreases Nu . Eu is increased as the inlet pressure is reduced, which the same behavior is observed in pressure drop, indicating that the pressure drop performance is larger when the inlet pressure is lower.

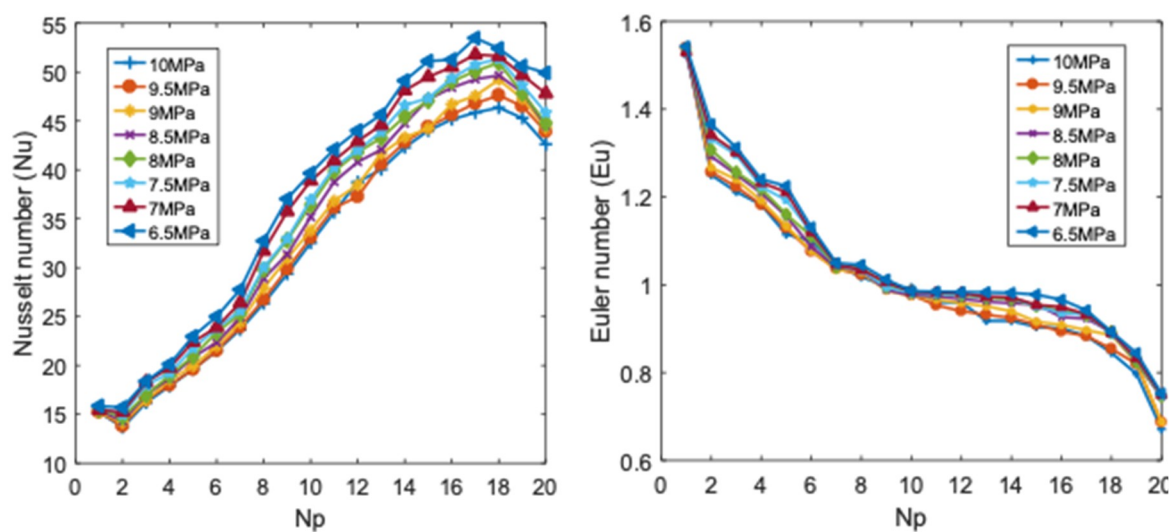


Figure 16. Effect of inlet pressure on Nu and Eu along the streamwise direction.

Although both Nu and Eu increase with a decrease in inlet pressure, Nu/Eu increases, as shown in Figure 17. This is because with the decrease of pressure, the increase rate of Nu is larger than that of Eu. Nu/Eu reaches its maximum at 6.5 MPa, indicating that supercritical LNG will have better heat transfer performance in PCHE at a lower inlet pressure.

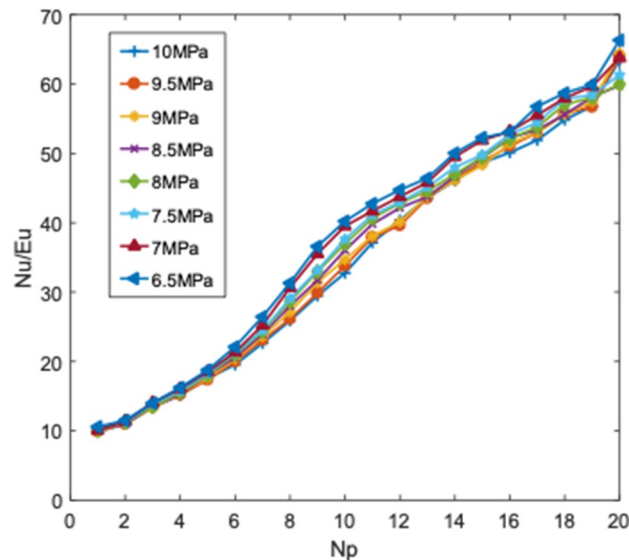


Figure 17. Effect of inlet pressure on Nu/Eu along the streamwise direction.

4. Conclusions

In this study, the flow and heat transfer characteristics of supercritical LNG in zigzag channel of PCHE are numerically investigated at different operating conditions. Some conclusions can be drawn as follows:

- (1) The local convection heat transfer coefficient rises and then falls along the streamwise direction, with the peak value appearing at the pseudo-critical temperature. The pressure drop also increases along the streamwise direction.
- (2) As the channel bend angle is increased, the local convection heat transfer coefficient and pressure drop rise, and so do the Nu and Euler numbers. The enhancement of heat transfer capability of supercritical LNG is mainly owed to increased turbulence. The increase of pressure drop is mainly due to the rising of velocity and the increase of flow resistance caused by the existence of vortices.
- (3) The local convective heat transfer coefficient and pressure drop increase significantly as the mass flux is increased due to the enhancement of turbulent flow. When the mass flux is increased by 2-fold, the local heat transfer coefficient rises by 1.4 times, and the pressure drop increases 3.3 times. The Nu increases as mass flux is increased. However, at the last third of the channel, Nu decreases as the mass flux is raised because of the decreased heat per unit volume absorbed by the LNG. This suggests that when the mass flux is raised, the heat transfer performance of the whole channel is better, but with the development of the fluid's flow, the local heat transfer performance is reduced at the last third of the channel owing to the reduction of heat-absorbed capacity by the unit volume fluid.
- (4) The improvement of heat transfer performance with bend angle depends on the mass flux. The supercritical LNG has better heat transfer performance when the bend angle is less than 15° when the mass flux ranges from $207.2 \text{ kg}/(\text{m}^2\cdot\text{s})$ to $621.6 \text{ kg}/(\text{m}^2\cdot\text{s})$, and improves at bend angles of 10° and lower compared to 15° at mass fluxes above $414.4 \text{ kg}/(\text{m}^2\cdot\text{s})$.
- (5) Before the pseudo-critical temperature, the local convective heat transfer coefficient changes little with the inlet pressure, while it increases when the temperature surpasses pseudo-critical

point. The pressure drop is reduced as the inlet pressure increases. Nu and EU decrease with increasing inlet pressure, while Nu/Eu reaches a maximum at 6.5 MPa. The results show that supercritical LNG has a better heat transfer performance in zigzag channel of PCHE at lower operating pressures.

Author Contributions: Conceptualization and supervision, Z.Z.; formal analysis and data curation, Y.Z.; validation, methodology and software, X.M., X.C., S.L., S.Y. and Z.Z.; writing—original draft preparation, Y.Z. and Z.Z.

Funding: The authors gratefully acknowledge that this work was supported by Jiangsu marine and fishery science and technology innovation and extension project (HY2017-8), Zhenjiang funds for the key research and development project (GY2016002-1) and National Key R&D Program of China (2018YFC0310400).

Conflicts of Interest: The authors declare no conflict of interest.

Nomenclature

T	Temperature (K)
P	Pressure (Pa)
L	length of channel (mm)
f	Fanning factor
v	Velocity (m/s)
Re	Reynolds number
h	Convective heat transfer coefficient ($W/(m^2 \cdot K)$)
Nu	Nusselt number
Eu	Euler number
C_p	Specific heat ($KJ/(kg \cdot K)$)
D_h	hydraulic diameter (m)
G	mass flux ($kg/(m^2 \cdot s)$)
ΔP	pressure drop (Pa)
ΔP_f	pressure drop due to friction (Pa)
ΔP_a	pressure drop due to acceleration (Pa)
τ	shear stress at the wall (Pa)

Greek symbols

μ	viscosity ($Pa \cdot s$)
ρ	density (kg/m^3)
λ	thermal conductivity ($W/(m \cdot K)$)

Subscript

w	Wall
b	Bulk mean
in	inlet
out	outlet

References

1. Pham, T.N.; Long, N.V.D.; Lee, S.; Lee, M. Enhancement of single mixed refrigerant natural gas liquefaction process through process knowledge inspired optimization and modification. *Appl. Therm. Eng.* **2017**, *110*, 1230–1239. [[CrossRef](#)]
2. Pu, L.; Qu, Z.G.; Bai, Y.H.; Qi, D.; Sun, K.; Yi, P. Thermal performance analysis of intermediate fluid vaporizer for liquefied natural gas. *Appl. Therm. Eng.* **2014**, *65*, 564–574. [[CrossRef](#)]
3. Xu, S.; Chen, X.; Fan, Z. Thermal design of intermediate fluid vaporizer for subcritical liquefied natural gas. *J. Nat. Gas Sci. Eng.* **2016**, *32*, 10–19. [[CrossRef](#)]
4. Pan, J.; Li, R.; Lv, T.; Wu, G.; Deng, Z. Thermal performance calculation and analysis of heat transfer tube in super open rack vaporizer. *Appl. Therm. Eng.* **2016**, *93*, 27–35. [[CrossRef](#)]

5. Han, C.-L.; Ren, J.-J.; Wang, Y.-Q.; Dong, W.-P.; Bi, M.-S. Experimental investigation on fluid flow and heat transfer characteristics of a submerged combustion vaporizer. *Appl. Therm. Eng.* **2017**, *113*, 529–536. [[CrossRef](#)]
6. Kim, J.H.; Baek, S.; Jeong, S.; Jung, J. Hydraulic performance of a microchannel PCHE. *Appl. Therm. Eng.* **2010**, *30*, 2157–2162. [[CrossRef](#)]
7. Chu, W.-X.; Li, X.-H.; Ma, T.; Chen, Y.-T.; Wang, Q.-W. Experimental investigation on SCO₂-water heat transfer characteristics in a printed circuit heat exchanger with straight channels. *Int. J. Heat Mass Transf.* **2017**, *113*, 184–194. [[CrossRef](#)]
8. Figley, J.; Sun, X.; Mylavarapu, S.K.; Hajek, B. Numerical study on thermal hydraulic performance of a Printed Circuit Heat Exchanger. *Prog. Nucl. Energy* **2013**, *68*, 89–96. [[CrossRef](#)]
9. Kim, W.; Baik, Y.-J.; Jeon, S.; Jeon, D.; Byon, C. A mathematical correlation for predicting the thermal performance of cross, parallel, and counterflow PCHEs. *Int. J. Heat Mass Transf.* **2017**, *106*, 1294–13022. [[CrossRef](#)]
10. Yoon, S.-Y.; O'Brien, J.; Chen, M.; Sabharwall, P.; Sun, X. Development and validation of Nusselt number and friction factor correlations for laminar flow in semi-circular zigzag channel of printed circuit heat exchanger. *Appl. Therm. Eng.* **2017**, *123*, 1327–1344. [[CrossRef](#)]
11. Ishizuka, T.; Kato, Y.; Muto, Y.; Nikitin, K.; Tri Lam, N. Thermal-hydraulic characteristics of a Printed Circuit Heat Exchanger in a supercritical CO₂ loop. *Nucl. React. Therm. Hydraul.* **2006**, *30*, 109–116.
12. Tsuzuki, N.; Kato, Y.; Ishiduka, T. High performance printed circuit heat exchanger. *Appl. Therm. Eng.* **2007**, *27*, 1702–1707. [[CrossRef](#)]
13. Ngo, T.L.; Kato, Y.; Nikitin, K.; Tsuzuki, N. New printed circuit heat exchanger with S-shaped fins for hot water supplier. *Exp. Therm. Fluid Sci.* **2006**, *30*, 811–819. [[CrossRef](#)]
14. Ngo, T.L.; Kato, Y.; Nikitin, K.; Ishizuka, T. Heat transfer and pressure drop correlations of microchannel heat exchangers with S-shaped and zigzag fins for carbon dioxide cycles. *Exp. Therm. Fluid Sci.* **2007**, *32*, 560–570. [[CrossRef](#)]
15. Kim, D.E.; Kim, M.H.; Cha, J.E.; Kim, S.O. Numerical investigation on thermal hydraulic performance of new printed circuit heat exchanger model. *Nucl. Eng. Des.* **2008**, *238*, 3269–3276. [[CrossRef](#)]
16. Zhao, Z.; Zhao, K.; Jia, D.; Jiang, P.; Shen, R. Numerical Investigation on the Flow and Heat Transfer Characteristics of Supercritical Liquefied Natural Gas in an Airfoil Fin Printed Circuit Heat Exchanger. *Energies* **2017**, *10*, 1828. [[CrossRef](#)]
17. Lee, S.Y.; Park, B.G.; Chung, J.T. Numerical studies on thermal hydraulic performance of zigzag-type printed circuit heat exchanger with inserted straight channels. *Appl. Therm. Eng.* **2017**, *123*, 1434–1443. [[CrossRef](#)]
18. Yoon, S.Y.; No, H.C.; Kang, G.B. Assessment of straight, zigzag, S-shape, and airfoil PCHEs for intermediate heat exchangers of HTGRs and SFRs. *Nucl. Eng. Des.* **2014**, *270*, 334–343. [[CrossRef](#)]
19. Kim, I.H.; No, H.C. Physical model development and optimal design of PCHE for intermediate heat exchangers in HTGRs. *Nucl. Eng. Des.* **2012**, *243*, 243–250. [[CrossRef](#)]
20. Huang, D.; Wu, Z.; Sunden, B.; Li, W. A brief review on convection heat transfer of fluids at supercritical pressures in tubes and the recent progress. *Appl. Energy* **2016**, *162*, 494–505. [[CrossRef](#)]
21. Kim, I.H.; No, H.C. Thermal-hydraulic physical models for a Printed Circuit Heat Exchanger covering He, He-CO₂ mixture, and water fluids using experimental data and CFD. *Exp. Therm. Fluid Sci.* **2013**, *48*, 213–221. [[CrossRef](#)]
22. Yu, X.; Yang, X.; Wang, J. Heat Transfer and Pressure Loss of Immediate Heat Exchanger. *Inst. Nucl. New Energy Technol.* **2009**, *43*, 256–259.
23. Sung, J.; Lee, J.Y. Effect of tangled channels on the heat transfer in a printed circuit heat exchanger. *Int. J. Heat Mass Transf.* **2017**, *115*, 647–656. [[CrossRef](#)]
24. Nikitin, K.; Kato, Y.; Ngo, L. Printed circuit heat exchanger thermal-hydraulic performance in supercritical CO₂ experimental loop. *Int. J. Refrig.* **2006**, *29*, 807–814. [[CrossRef](#)]
25. Jeon, S.; Baik, Y.-J.; Byon, C.; Kim, W. Thermal performance of heterogeneous PCHE for supercritical CO₂ energy cycle. *Int. J. Heat Mass Transf.* **2016**, *102*, 867–876. [[CrossRef](#)]
26. Higashi, Y. NIST Thermodynamic and Transport Properties of Refrigerants and Refrigerant Mixtures (REFPROP). *Netsu Bussei* **2000**, *14*, 1575–1577.
27. Kwon, J.G.; Kim, T.H.; Park, H.J.; Cha, J.E.; Kim, M.H. Optimization of airfoil-type PCHE for the recuperate of small scale Brayton cycle by cost-based objective function. *Nucl. Eng. Des.* **2016**, *298*, 192–200. [[CrossRef](#)]

28. Han, C.L.; Ren, J.J.; Dong, W.-P.; Bi, M.-S. Numerical investigation of supercritical LNG convective heat transfer in a horizontal serpentine tube. *Cryogenics* **2016**, *78*, 1–13. [[CrossRef](#)]
29. Xu, X.; Ma, T.; Li, L.; Zeng, M.; Chen, Y.; Huang, Y.; Wang, Q. Optimization of fin arrangement and channel configuration in an airfoil fin PCHE for supercritical CO₂ cycle. *Appl. Therm. Eng.* **2014**, *70*, 867–875. [[CrossRef](#)]
30. Zhao, Z.; Zhang, X.; Zhao, K.; Jiang, P.; Chen, Y. Numerical investigation on heat transfer and flow characteristics of supercritical nitrogen in a straight channel of printed circuit heat exchanger. *Appl. Therm. Eng.* **2017**, *126*, 717–729. [[CrossRef](#)]
31. Yang, J.G.; Wu, H. Explicit Coupled Solution of Two-equation k- ω SST Turbulence Model and Its Application in Turbomachinery Flow Simulation. *Acta Aeronaut. ET Astronaut. Sinaica* **2014**, *35*, 116–124.
32. Ren, Y.; Liu, H.L.; Shu, M.H. Improvement of SST k- ω SST Turbulence Model and Numerical Simulation in Centrifugal Pump. *Trans. Chin. Soc. Agric. Mach.* **2014**, *43*, 123–128.



© 2019 by the authors. Licensee MDPI, Basel, Switzerland. This article is an open access article distributed under the terms and conditions of the Creative Commons Attribution (CC BY) license (<http://creativecommons.org/licenses/by/4.0/>).